ELSEVIER

Physica D 89 (1995) 151–168

PHYSICA D

Chaos in a variable mass relaxation oscillator model for the leaky tap

Gerardo I. Sánchez-Ortiz[a,1], Alvaro L. Salas-Brito[b,2]

[a] *Department of Computing, Imperial College, London SW7 2BZ, UK*

[b] *Laboratorio de Sistemas Dinámicos, Departamento de Ciencias Básicas, Universidad Autónoma Metropolitana Azcapotzalco, Apartado Postal 21-726, Coyoacán 04000, D.F., México*

Received 6 September 1994; revised 8 March 1995; accepted 25 May 1995
Communicated by H. Flaschka

Abstract

A variable-mass relaxation oscillator model for the behaviour of the leaky tap is numerically investigated. Different regions of its three dimensional parameter space have been searched and interesting dynamical behaviour has been found. The dynamics of the system is thoroughly characterized using projections of phase space trajectories, 2 and 3 dimensional time-delay plots, power spectra, Lyapunov exponents, Hausdorff and correlation dimensions and bifurcation diagrams. Dynamical variables obtained from the model, like drop masses, velocities and drip-intervals, are used for reconstructing attractors. We found several periodic, intermittent and chaotic attractors. We conclude that the rich dynamics of the model investigated represents an improvement in describing the experimentally observed behaviour of the actual dripping faucet system.

PACS: 02.70+d; 47.20.Tg; 03.20.+i
Keywords: Dripping faucet models; Relaxation oscillator; Intermittent behaviour; Strange attractors

1. Introduction

During the past decade much effort has been devoted to the study of the onset of chaotic behaviour in non-linear systems [1–7]. One of the prototypical examples of dissipative systems where this transition occurs is the dripping faucet of which several experimental investigations have been reported [8–11]. The quantity measured in these studies is the time interval between successive drop detachments, the so-called *drip interval*, which has been used to reconstruct the seemingly chaotic attractors of the system. These studies have shown that this apparently trivial system exhibits very complex behaviour, ranging from the simply periodic to what appears to be strange attractors with varying degrees of complexity [12–14].

However, little has been done for modelling the dynamics behind the dripping faucet behaviour. The only attempts we know are the one-dimensional feedback-loop model of Austin [14], the electric analogue used by Bernhardt [15], and the variable-mass oscillator model of Shaw [8]; but, as far as we know, only Bernhardt's model has been subjected to a systematic

[1] Work partially done at: Departamento de Física Teórica, Instituto de Física, Univerisdad Nacional Autónoma de México, D.F., México.

[2] Work partially done while affiliated with Laboratorio de Cuernavaca, Instituto de Física, UNAM.

SSDI 0167-2789(95)00209-X

investigation. In particular, Shaw's model has never been tested to find out whether it possesses strange attractors and hence if it is a suitable model for the dripping faucet behaviour, albeit some evidence for the existence of attractors has been obtained by using analogue simulations [8,9]. This is surprising since the leaky tap has been even considered as the starting point for developing a non-linear model for magnetospheric processes [16].

The purpose of this work is to describe an investigation of a modified oscillator model. As it turns out, the change done to Shaw's model bring it closer to the behaviour of an actual leaky tap. With the intention of obtaining evidence of strange and chaotic behaviour, we look for attractors in different regions of the model's space of parameters, we analyse them qualitatively and also quantitatively by determining their Lyapunov exponents and Hausdorff and correlation dimensions. Results for the periodic and the chaotic behaviour of the model reveal the similarities and dissimilarities of its dynamics with that of the real dripping system. We present tables showing characteristics of some of the attractors and their distribution in the space of parameters of the model. We also show bifurcation diagrams of some regions of this space.

2. The variable-mass oscillator model

In 1984 Shaw proposed a set of differential equations for modelling the dripping behaviour of a leaky tap. The equations are based on the image of a drop hanging from a nozzle and eventually falling from it, as a kind of one-dimensional oscillator [17,18] in which the cohesive force in the liquid (basically the surface tension σ) is modelled by the elastic force in the oscillator. The oscillator can be thought as driven by the pushing effect of the water flowing into the drop and by its own increasing weight. To model the flow of water feeding the hanging drop before the detachment, the bob's mass is assumed to increase at a constant rate. To maintain the simplicity of the model, it is further assumed that the breaking-off time for each drop occurs when the oscillator reaches a certain prefixed length l —which may be thought of as analogous to the behaviour of an actual drop beyond the meniscus length. The internal dissipative forces are represented by a velocity dependent term.

With the above considerations in mind, we may see that the (dimensionless) first-order equations of the model are

$$\frac{dx}{dt} = v, \tag{1}$$

$$\frac{dv}{dt} = \frac{1}{m}(x + v) - g, \tag{2}$$

$$\frac{dm}{dt} = f, \tag{3}$$

where x, v and m are to be taken as the coordinates in the phase space of the model. We may think of x, v and m as the position, velocity and mass of the drop respectively, g as the external force, and f as the flow rate. Eqs. (1)–(3) are to be solved together with the following proviso for the detachment of the drop when the position variable reaches a certain value — in the non-dimensional coordinates we normalize to unity the critical value $x_c = 1$:

$$\text{When } x = 1, \text{ then } m(t + dt) = m(t) - \Delta m, \tag{4}$$

where

$$\Delta m = hm(t)v(t). \tag{5}$$

Here we calculate the mass of the falling drop, Δm, where h is another constant and by $t + dt$ we mean an instant after the system reaches $x = x_c$ (dt is taken as the integration step when solving numerically the equations). We must remember that the dimensionless parameters f, g and h have algebraic relationships with the constants and parameters of the original equations for a variable-mass damped oscillator driven by a constant force. Therefore varying the parameter akin to an external force (g), for example, might have a complicated physical analogy if we think in terms of the oscillator.

Notice that whereas Shaw assumed Δm to be proportional to v only, we made it dependent also on the available mass at that moment. With this change the model gains a closer correspondence with the actual

experiment as well as a sort of control mechanism of the minimum mass of the drop, m, avoiding thus an excessively large value of the force in Eq. (2) and therefore permitting greater flexibility in the selection of parameters. While the change keeps the model simple, our results show that it makes much richer the dynamics of the system. As a relaxation oscillator is fundamental for understanding the behaviour of the leaky tap, the discontinuity imposed on the model is a very important ingredient of the model since it generates both a threshold and a rapid depletion of the mass accumulated in the oscillator.

The dynamics of the model was investigated by numerically integrating Eqs. (1)–(3) with an algorithm which takes into account the existence of the discontinuity. At the moments when the dripping occurs four data were always stored: the drip interval T_n (where n is the drop number), the mass of the drop M_n, the velocity V_n at the moment of the detachment, and the mass which remains hanging from the nozzle, Q_n (which can be computed as $Q_n = Q_0 + f\sum_{i=1}^{n} T_i - \sum_{i=1}^{n} M_i$). From each of the data series, the underlying attractors are reconstructed using time-delay plots (also called return maps) in analogous fashion to what is done with the drip intervals of experimental results [9,10,13,14]. Although as far as we know previous works have only dealt with time intervals as a result of the difficulty to measure other quantities experimentally, recent studies [26] analyse certain characteristics of the system by making estimations of the drops' masses (sizes) from time measurements. In this work we present most of the results as reconstructions made from time intervals to enable comparisons with other studies, but we also show that the analysis of the other system variables can provide with complementary information.

The model is studied in various regions of its 3-dimensional parameter space (f, g, and h). A summary of the distribution of attractors is presented in Table 1, while a detailed analysis of some regions is shown with bifurcation diagrams (Fig. 12). Power spectra, maximal Lyapunov exponents, Hausdorff and correlation dimensions were calculated for some of the attractors (Table 2).

3. Results

Plots of the x–v ($v \equiv \dot{x}$) projections of the phase space trajectories were done simultaneously with the integration of the equations for each set of values of the parameters and initial conditions. The search for attractors was done in the region of the space of parameters bounded by $0.05 < f < 2$, $0.1 < g < 1$, $5 < h < 11$ avoiding the zones where the system was "saturated". For example, when f was large and h small, the mass was still too big after the detachment of the drop and the upward force of the spring was not enough to counteract the weight, so the system could not "go up" again (this behaviour may be thought of as analogous to the situation in which the falling of drops becomes a continuous stream). As a general procedure several sets of starting conditions were tested looking for different coexisting attractors at the same parameter values, but these were never found.

3.1. Periodic attractors

For most of the domain of parameters investigated, the system shows a very quick convergence to cyclic attractors of period 1, 2, 3, 4, 5, 8 or 12. The x–v projected phase trajectories, time-delay plots of its drip intervals (T_n vs. T_{n+1}), and the corresponding power spectrum of a period 5 attractor, are shown in Fig. 1 together with a time-delay plot of a period 8 attractor. To illustrate the process of convergence towards the attractor, Fig. 1b exhibits the transient state as small dots and the final state (the attractor) as big ones (except for some figures where we specify the opposite, transient states were excluded from the plots to avoid clutter). The power spectrum of Fig. 1c shows the peak at the frequency $\frac{1}{5}$ and its harmonic. Due to the way we sampled the data, the maximum frequency displayed in all power spectra corresponds to $\frac{1}{2}$ (the Nyquist frequency). As power spectra computed from any of the series of data taken (i.e. masses, velocities, etc.) showed the same general shape, we only present the ones calculated from the drip interval series.

Between certain parameter values where the system has cyclic attractors with periods 1 and 2, a third value

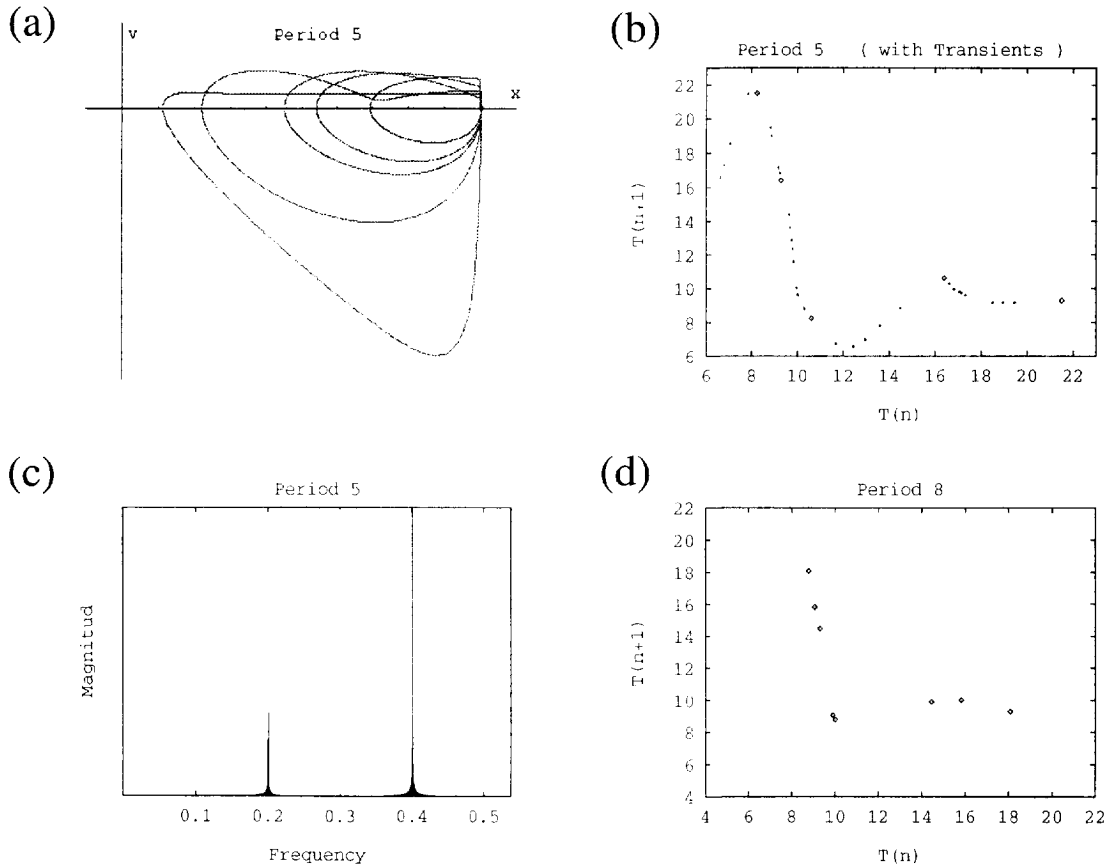

Fig. 1. (a) x–v projected phase space trajectory of a period 5 attractor (without transients). Every time a loop was completed, a part of the mass dripped from the system and the data were stored. (b) Poincaré map of the drip intervals of the same period 5 attractor (big dots) and its transients (small dots). (c) Power spectrum of the period 5 attractor. The maximum frequency displayed is $\frac{1}{2}$, the Nyquist frequency for this data series. (d) Poincaré map of the drip intervals of a Period 8 attractor. Notice that the shape of these reconstructed attractors evolves towards that of attractor ECGPAR shown in Fig. 8b. This a result of the relatively smooth change of the system with the variation of the parameters that can be observed in Table 1.

was sometimes found where the system appeared to be in a period 1 attractor, but the trajectory eventually splitted into two well defined cycles, i.e. it was only a transient state for a period 2 attractor. The same kind of transitions were found from other transient states which could be mistaken with a periodic attractor, but which eventually ended in an attractors with a different period ($1 \rightarrow 2$, $2 \rightarrow 1$, $2 \rightarrow 4$ and $4 \rightarrow 2$). Fig. 2 shows some of these attractors and their apparently periodic transient states. Notice that the broad peak at the frequency $\frac{1}{4}$ of the power spectrum of Fig. 2b indicates the system does not visit exactly the same four points, but some values in their neighbourhoods. In the same way, the presence of all the other frequencies between this peak and the high one at $\frac{1}{2}$, are the result of the evolution of the system from a period 4 to a period 2 behaviour (the bifurcation diagrams of Figs. 12e and 12f discussed below show the smooth way in which the system passes from one periodic attractor to the next).

3.2. Chaotic attractors

3.2.1. PAR

Fig. 3 shows time-delay plots made of drip intervals, masses and velocities of a strange attractor with 5 well defined regions where the density of points is notoriously higher. All reconstructions show a thin (one-

Table 1
Attractors of the system in some regions of the space of parameters

Parameters			Attractor
f	g	h	
0.40	0.32	10	period 1
0.35	,,	,,	,, 1
0.3425	,,	,,	,, 2
0.34	,,	,,	PAR
0.338	0.325	,,	PAR-INT
0.33	0.32	,,	period 3
0.30	,,	,,	,, 3
0.20	,,	,,	,, 4
0.19	,,	,,	,, 4
0.18	,,	,,	,, 8
0.17	,,	,,	,, 5
0.15	,,	,,	,, 5
0.14	,,	,,	ECGPAR
0.11	,,	,,	,,
0.09	,,	,,	,,
0.09	0.34	7	ECG
0.10	,,	,,	,,
0.104905	,,	,,	period 12 window
0.11	,,	,,	ECG
0.115	,,	,,	,,
0.112	,,	,,	,,
0.112470	,,	,,	intermittent ECG
0.113	,,	,,	period 2
0.12	,,	,,	,, 2
0.20	,,	,,	,, 2
0.35	,,	,,	,, 2
0.40	,,	,,	,, 1
0.50	,,	,,	,, 1
1.00	,,	,,	,, 1
0.10	0.36	7	period 2 → ECG-INT
,,	0.40	,,	period 2
,,	0.45	,,	,, 2
,,	0.50	,,	,, 4 → 2
,,	0.55	,,	,, 4
,,	0.65	,,	,, 4
,,	0.72	,,	,, 2 → 4
,,	0.82	,,	,, 1 → 2
,,	0.8340	,,	long transient period 1 → 2
,,	0.85	,,	period 2 → 1

dimensional) line, and for the drip intervals (Fig. 3c) the 5 regions are contained in a parabolic curve (reason why we refer to it with the nickname PAR). Notice that due to the order in which the different regions of the attractor are visited, drawn with lesser magnification this attractor could be mistaken with a cyclic attractor of period 5 – this also happens in experimental data [19]. A very thick peak around the frequency $\frac{1}{5}$ of the power spectrum (Fig. 3b), and the presence of relatively high peaks in all frequencies show the heterogeneous behaviour of this 5 bands strange attractor. Three dimensional time-delay plots show the strong dependence of one drop on the two previous ones. In Fig. 3f we can appreciate that the time-delay plot of the velocities introduces a fold of the curve onto itself that can not be seen in the other reconstructions. This is an example of the rare cases in which one of the reconstructions shows structural details which are not obvious in the others.

3.2.2. ECG

Fig. 4 exhibit the chaotic attractor ECG (the nickname comes from the resemblance to an electrocardiogram). Fig. 4a shows a projection on the plane x–v of the phase space trajectory of about a hundred drops, while Fig. 4b presents a series of 35,000 drip intervals of the same attractor. The power spectrum computed from 130,000 data (Fig. 4c) shows a peak around the frequency $\frac{1}{2}$ corresponding to the dense accumulation of points in the neighbourhood of two values on the attractor shown in Fig. 4b (the system goes from one of these regions to the other, behaving like a "coarse" period 2 attractor). The other two protuberances next to the frequencies $\frac{1}{4}$ and $\frac{1}{8}$ may indicate the same phenomena described above but now for a somewhat hidden "coarse" period 8 behaviour.

The time-delay plot of 300,000 drip intervals of the ECG attractor and magnifications of some of its regions are presented in Fig. 5. The successive enlargements of a region shown in Figs. 5c and d exhibit some of the substructure of the set. This kind of behaviour was found in different parts of other strange attractors and it is responsible for the fractal dimensions larger than one. The self-crossing plots are a remainder of the fact that the nth data point depends not only on the $(n-1)$th, but also on other previous values. Two and three dimensional time-delay plots of the series of drip intervals and masses are shown in Fig. 6. Notice that the reconstruction for the masses, in spite of the complex separation of its lines, still presents the kind of substructure shown for the drip intervals. The hanging masses (Q_n) and plots of mixed dynamical

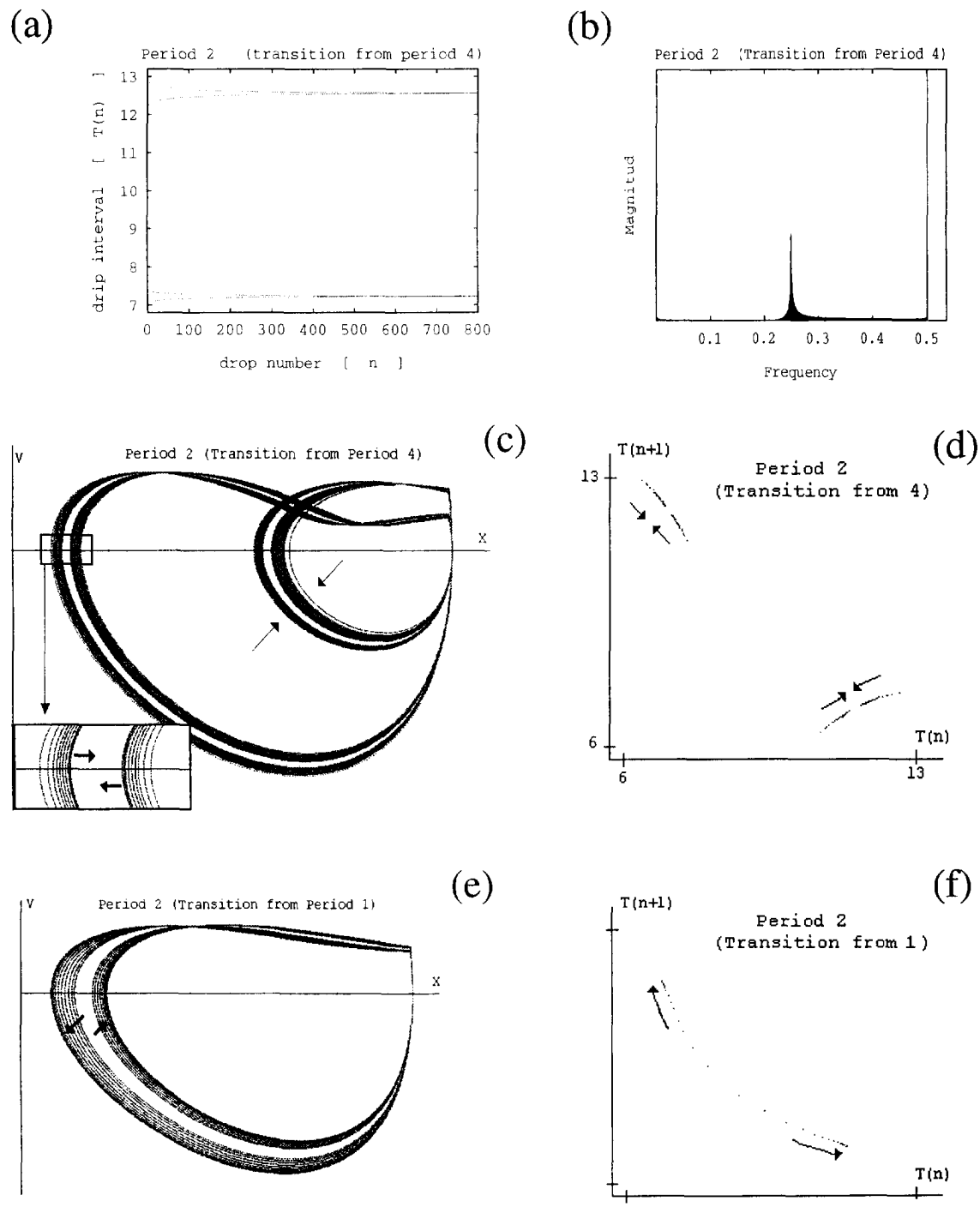

Fig. 2. (a) Series of drip intervals of a period 2 attractor with transients moving from a period 4 attractor behaviour. (b) Power spectrum of data shown in (a). In order to show the small peak at frequency $\frac{1}{4}$ in a regular size, peak at frequency $\frac{1}{2}$ is not shown complete. (c) x–v projected phase space trajectory of the first 50 drops (loops) of the period 2 attractor reconstructed in (a). Arrows (except for that showing the magnification of a region) show the direction in which transient trajectories are translating. (d) Poincaré map of the drip intervals of figure (a). (e) x–v projected phase space trajectory of the first some 25 drops of the period 2 attractor with transients moving from a period 1 attractor behaviour. (f) Poincaré map of the drip intervals reconstruction of the attractor of (e).

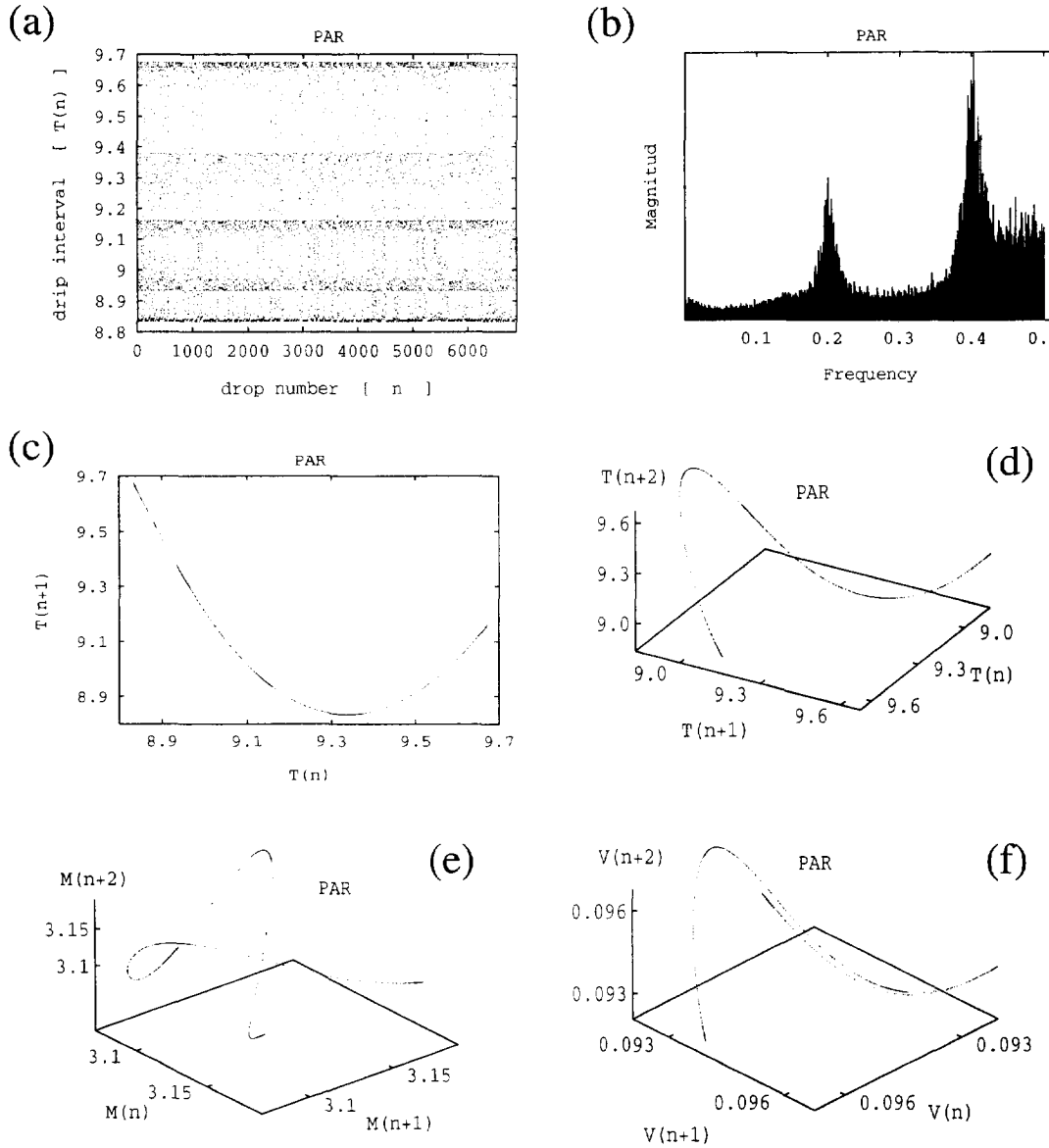

Fig. 3. (a) Series of drip intervals of the strange attractor PAR. Notice the 5 bands with higher density of dots. (b) Power spectrum of data shown in (a). The spectrum shows the heterogeneous behaviour of rough period 5 (broad peaks at frequencies $\frac{1}{4}$ and $\frac{1}{2}$) within a strange attractor (components in all the frequency range). (c) Poincaré map of the drip intervals of figure (a), showing a parabolic "thickless" line. (d), (e) and (f) are 3-dimensional Poincaré maps of the attractor PAR reconstructed with drip intervals, masses and velocities, respectively. Notice that only the series of velocities present a folding of the curve onto itself.

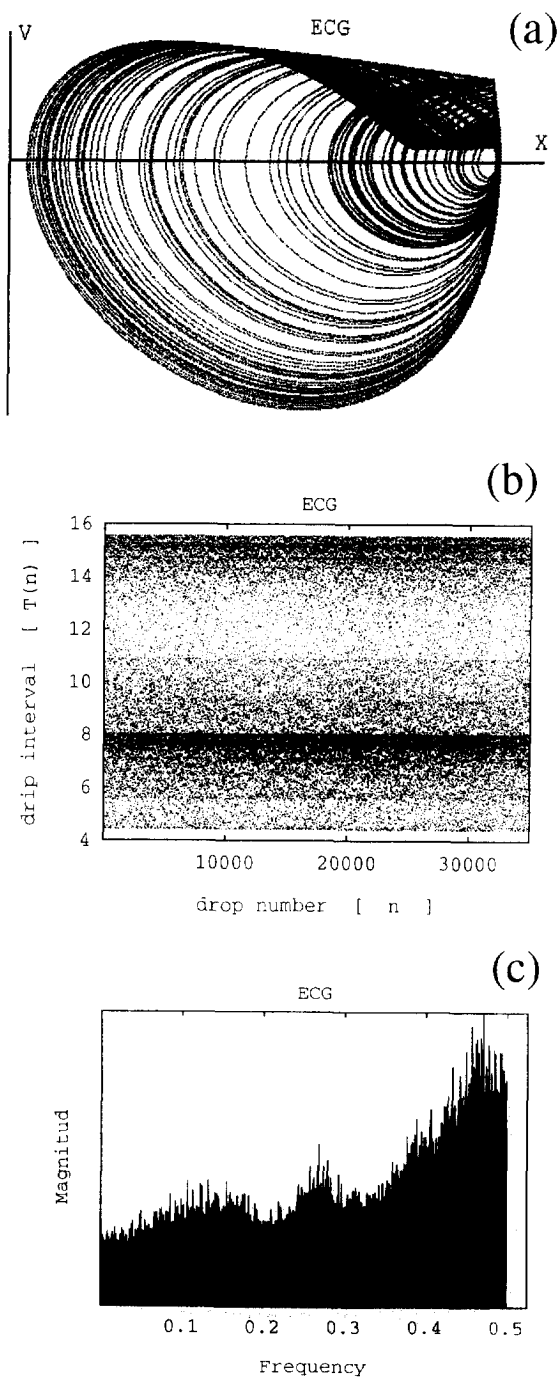

Fig. 4. (a) x–v projected phase space trajectory of about 100 drops of the ECG attractor. (b) Series of drip intervals of the strange attractor ECG. Notice the 2 bands with higher density of dots. (c) Power spectrum of attractor ECG. Protuberances appear in the neighbourhood of frequencies $\frac{1}{8}$, $\frac{1}{4}$ and $\frac{1}{2}$.

variables of the system at the breaking-off time are shown in Fig. 7.

3.2.3. *ECGPAR*

Figs. 8 and 9 show reconstructions made from data of attractor ECGPAR (the name was given because the values of its parameters are a mixture of both attractors ECG and PAR). Notice the huge difference in the complexity of the plots for the hanging mass and the velocity, although both are reconstructions of the same chaotic attractor. The evident heterogeneous distribution of points in this curve is characterized below by the correlation dimension. This is a good example of the accuracy with which this model reproduces some of the attractors found in experiments with the real dripping system (see Fig. 12b of Ref. [25]). Fig. 9f was included to show the partial loss of correlation between one drop and its third "generation" (nth vs. $(n+3)$th).

3.3. *Intermittence*

3.3.1. *ECG-INT*

Varying the value of the parameters from those of the ECG attractor, a region of the graph T_n vs. T_{n+3} seems to approach tangentially the identity line leading to a curious kind of intermittent behaviour. Plots of the drip intervals and some windows of this attractor (ECG-INT), together with their corresponding power spectra are displayed in Fig. 10. The system alternates between three different states in a chaotic fashion: a relatively long state (up to 100 drops), where it behaves like in a cyclic attractor of period 3, another shorter state (typically of about 20 drops) where the system appears to be in cyclic attractor of period 2 in which the two time intervals gradually got shorter ("contracting"), and another state of variable duration where the system visits points on the curve either in an irregular manner (chaotically) or with a brief cyclic behaviour with a high period (like 6, for example). In Fig. 10b we can see a succession of several "contracting" period 2 states, a period 3, a period 2, a period 6, and then an alternation of period 2 and irregular behaviour. Both spectra shown in Fig. 10, exhibit high peaks around frequencies $\frac{1}{2}$ and $\frac{1}{3}$, but they

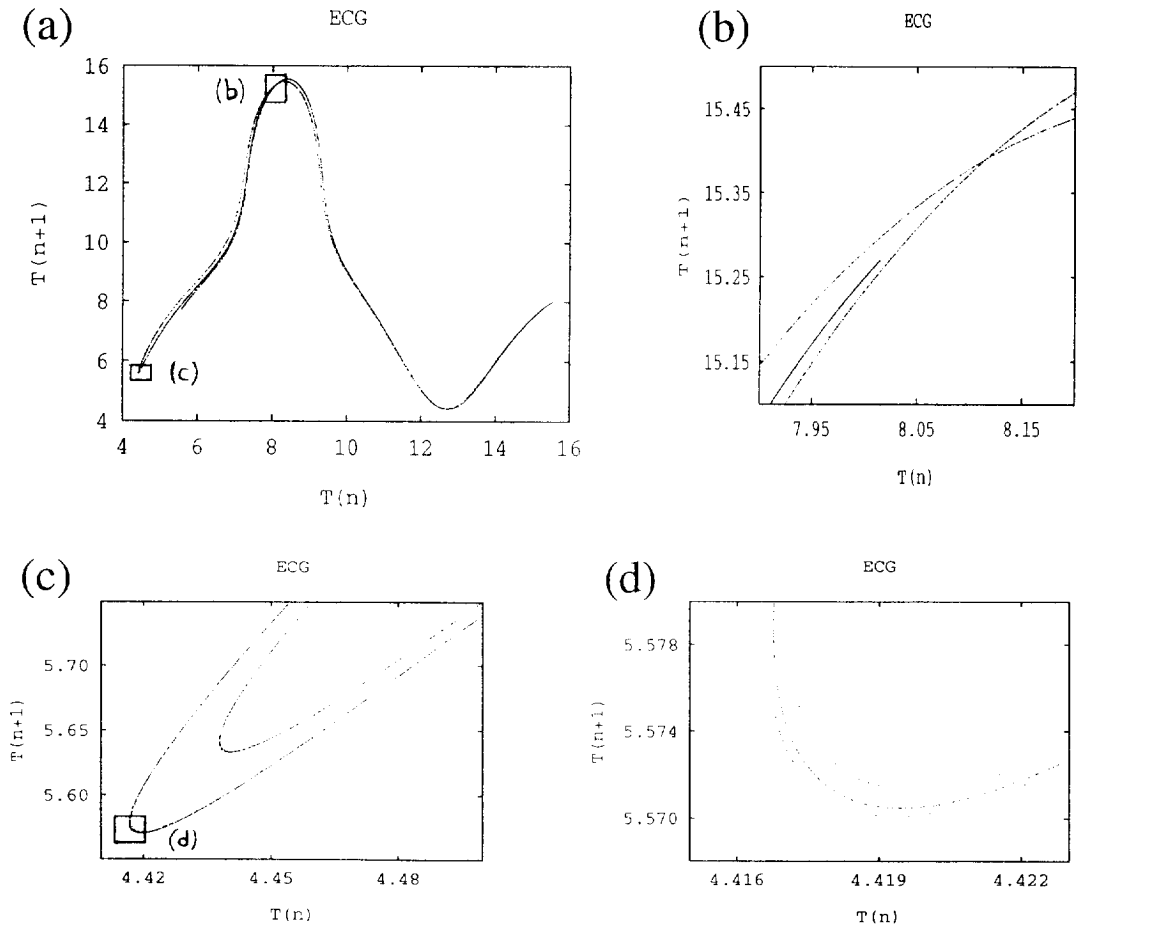

Fig. 5. (a) Poincaré map of the drip intervals of the attractor ECG shown in Fig. 4. (b) and (c) are the respective enlargements of regions W1 and V1 of (a), showing the substructure of the set present in several other regions. (d) Enlargement of region V2 of (c). 300,000 data were used for reconstructing the attractor that is partially shown here.

are enhanced in that of Fig. 10f computed from data of Fig. 10b. The continuum of frequencies is a manifestation of chaotic behaviour (the positive Lyapunov exponents found below reinforce this idea), while the other main peaks probably are the result of the rare and brief cyclic states with high period numbers. More tangent intermittence of attractor ECG leading to tangent bifurcations is discussed with the scan of parameters.

3.3.2. *PAR-INT*

The attractor PAR-INT of Fig. 11 was found by changing a little the value of the parameters from those of the attractor PAR. In Fig. 11a the strange kind of cyclic behaviour of this intermittent attractor can be clearly seen. This attractor is more interesting since the "cyclic" regions are in fact 5 wide bands visited successively (like in a period 5 attractor), but the exact positions inside them remain chaotic. The intermittent behaviour manifest when once in a while the attractor leaves these bands to visit points in between. The broad peaks of the power spectrum are a consequence of the wide of the bands, while the presence of all the other frequencies in a smaller proportion are due to the windows with irregular movement. The behaviour, and therefore the spectrum, is somewhat similar to that of the period 5 and the PAR attractors, shown in Figs. 1c and 3b, respectively.

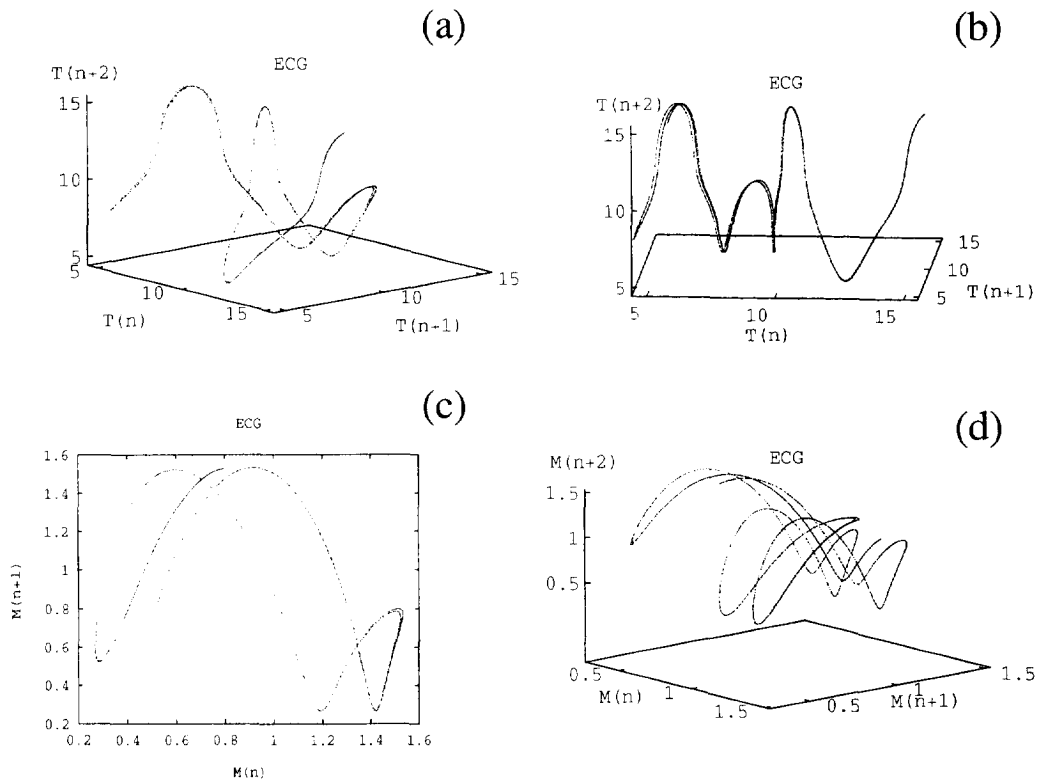

Fig. 6. (a), (b) and (d) are 3-dimensional Poincaré maps of the attractor ECG reconstructed from drip intervals (2 different views) and masses, respectively. (c) Poincaré map (in 2 dimensions) of the series of masses of attractor ECG. This is a projection of the 3-dimensional map of (d). Notice that by construction, 2 of the 3 projections onto planes of the 3-dimensional maps must have exactly the same shape. All curves present the same kind of substructure shown in Fig. 5.

3.4. Scan of parameters

Using bifurcation diagrams, Fig. 12 exhibits the behaviour of the system for some regions of the space of parameters. In Fig. 12a we variate parameter f and observe the transition from the chaotic attractor ECG to a period 2 and then period 1 attractors. Fig. 12b show with more detail the region of the transition from attractor ECG to period 2. We can appreciate the way in which the higher density zones of the attractor evolve with the change of f, abruptly contracting to the 2 values of the cyclic attractor. Fig. 12d shows in detail the way in which the transition occurs. We examined this behaviour and discovered that, as f increases, the attractor ECG becomes intermittent and gradually stabilizes into a period 2 attractor. Notice that the plot has 300 dots per vertical line, of which, most are concentrated in 2 dense bands that correspond to the laminar stage of this intermittent version of the ECG attractor. The few dots outside from these bands correspond to the short escapes from the tangential region. As f increases, these bursts become less frequent. A second return map of the time intervals (T_n vs. T_{n+2}) confirmed that this intermittent behaviour correspond to a tangent bifurcation.

Fig. 12c shows in detail an irregular section of Fig. 12b. Here we can appreciate how attractor ECG gives way to period 12 attractors in an irregular and alternated manner. This diagram also makes clear that in this region, attractor ECG has a set of definite values (those of the period 12 attractor) and sometimes intervals (or bands, as seen in Fig. 4b) visited more often than the rest. When looking carefully at Fig. 12b, we can track the evolution of this values as the parameter

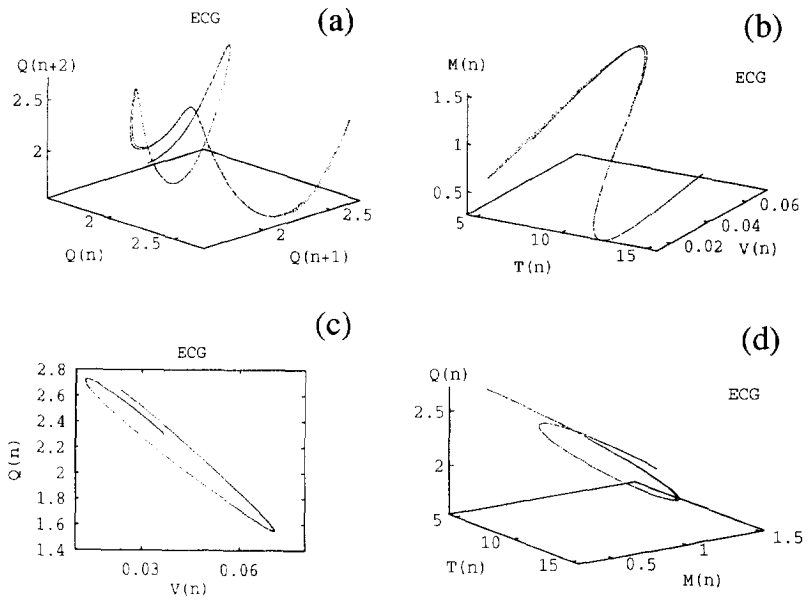

Fig. 7. (a) 3-dimensional Poincaré map of the attractor ECG reconstructed from the hanging masses (after the moment of the detachment). (b) 3 dimensional plot of the drip interval, mass and velocity of each drop of attractor ECG. (c) 2 dimensional plot of the hanging mass and the velocity of each drop of attractor ECG. (d) 3 dimensional plot of the drip interval, mass and hanging mass of each drop of attractor ECG. Notice that these plots give us information about the evolution of the states of the system.

f changes (for example those values of the period 12 attractor can be seen as curves of different shades in Fig. 12b).

In Fig. 12e we can follow the succession of attractors ECG, period 2, 4, 2 and 1 when increasing parameter g. A blow-up of the transition from period 2 to 1 (Fig. 12f) illustrates a pitchfork bifurcation and the behaviour described in Fig. 2. This diagram was made eliminating the first 100 time intervals for each value of the parameter g, and plotting the next 200. For some values of g this is enough to clear all transient states, but in the regions with a very thick curve, transient states last more and we can see a single value of the time intervals in their evolution towards 2 well differentiated values. Table 1 shows a summary of the behaviour of the system for various sets of parameters.

3.5. *Hausdorff and correlation dimensions*

In order to quantify the strangeness of some of the attractors described above we evaluated their Hausdorff and correlation dimensions using the method described by Grassberger and Procaccia [20,21] with series of about 130, 000 data. Table 2 shows the values found for the series of drip intervals and masses of these attractors. The different values of both dimensions obtained for a single series of data describe the distribution of points inside the attractor: for an homogeneous distribution the value of the correlation dimension equals that of Hausdorff, while for heterogeneous distributions the correlation value will always be smaller.

3.6. *Largest Lyapunov exponents*

Due to the difficulties associated with this kind of data and to the discontinuity present in the equations of the system, the largest Lyapunov exponent was calculated in two ways, one using the system equations and other using the series of data. From the system equations we let a difference vector evolve [22] carefully handling the discontinuity [23], and we used it to evaluate the exponent while integrating the equations, arriving to an approximate value certainly above zero. On the other hand, using the series of data of the reconstructed attractors with the method of Wolf [24]

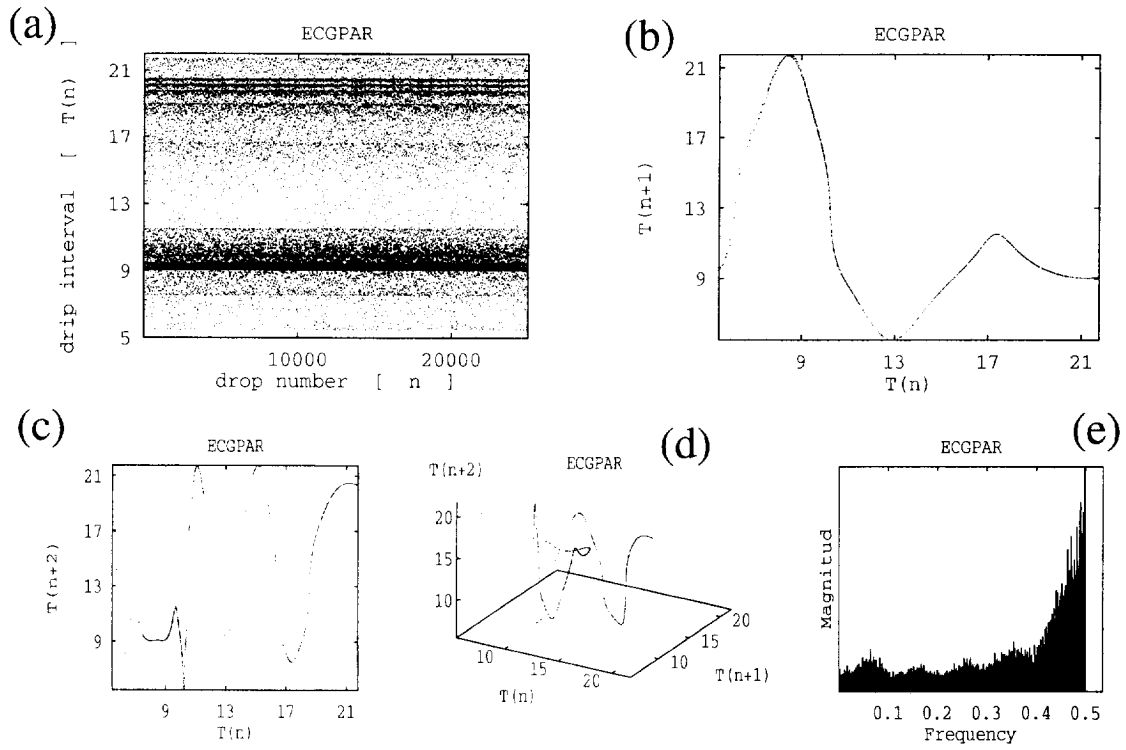

Fig. 8. (a) Series of drip intervals of the attractor ECGPAR. Notice that the several bands with higher density of dots are mostly grouped in two regions. (b) Poincaré map of the drip intervals of figure (a). (c) Plot of the drip intervals of (a) against the second following drip interval. This is a projection of the curve shown in the next plot. (d) 3-dimensional Poincaré map of the data of (a). (e) Power spectrum of data shown in (a). In the same way that we mentioned for the previous attractors, protuberances in this spectrum might be closely related to the number of bands present in (a).

we obtained the values shown in Table 2. These positive values together with the non-integer values of the dimensions offer a very strong numerical evidence of the existence of strange chaotic attractors in the oscillator model for the leaky tap.

4. Discussion

We studied the dynamics of an oscillator model for the leaky tap and found it to be very rich. Cyclic and strange attractors of the system were analysed with qualitative and quantitative methods, and evidence for chaos has been found. Our results show that the system of equations (1)–(5) provide a reasonable model for the dripping system. We believe the modification to Eq. (5) is an important ingredient in the improvement of the model.

Since not all the analysis presented here has an equivalent among the experiments for the real leaky tap, we focussed on some of our results and observed that the model reproduces many qualitative characteristics of the real system. Various experimental studies [10–12] have reported cyclic attractors of period 1, 2 and 4, and the unexpected periods 3 and 5 [12,25], all of them also found in the model. The transitions of periods $1 \leftrightarrow 2$, and $2 \leftrightarrow 4$ as well as the tangent bifurcations and the intermittence observed in the model have also a counterpart in the experiments of the real system [25]. We consider the similarities in the intermittence phenomena found (tangent intermittence and alternation between chaos and cyclic behaviour of various periods) as a strong link between both systems. The strange attractors ECG and PAR are very

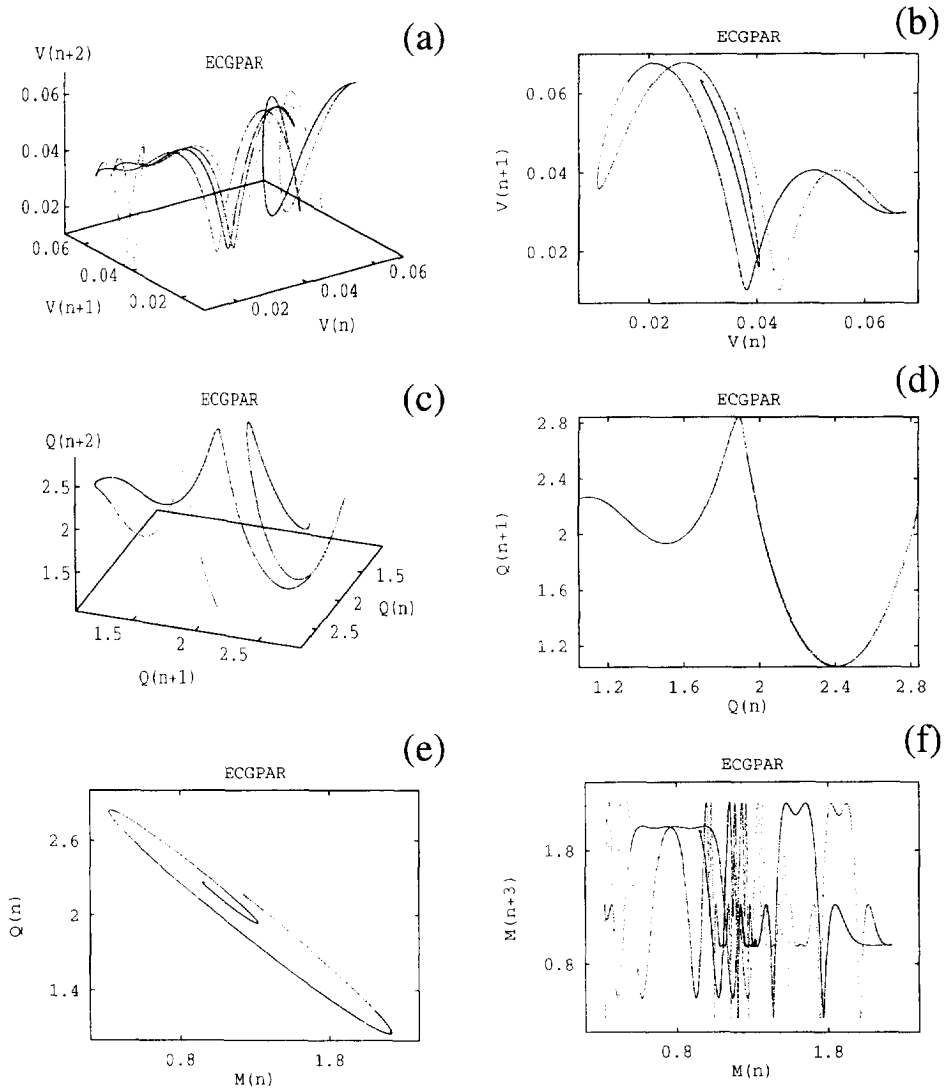

Fig. 9. (a) 3-dimensional Poincaré map of the attractor ECGPAR reconstructed from the velocities. (b) Poincaré map of the velocities of the same attractor (projection of (a)). (c) 3-dimensional Poincaré map of the hanging masses of attractor ECGPAR. (d) Projection of (c). (e) 2 dimensional plot of the mass and the hanging mass of each drop of attractor ECGPAR. (f) Plot of the masses of attractor ECGPAR against the third following mass. Notice that the highly complicated curve shows the quick loss of correlation between data.

similar to some others found experimentally [9–11]. Complex shaped attractors found in experiments with reduced noise conditions like that shown by Sartorelli et al. (Fig. 12b of Ref. [25]), are very closely matched by attractors in our model (see attractor ECGPAR, Fig. 8b).

Inversely to what is generally thought to happen with the leaky tap, increasing the flow parameter of the model makes the system pass from a periodic to a chaotic regime. Results for the real drop system show the same kind of behaviour [25]. However, a difference between both systems is the thickness of the time-delay plots of the attractors due to the noisy experimental systems and to the difficulties for counting neither more nor less drops than there are (optical detectors in the experiments frequently cannot count too

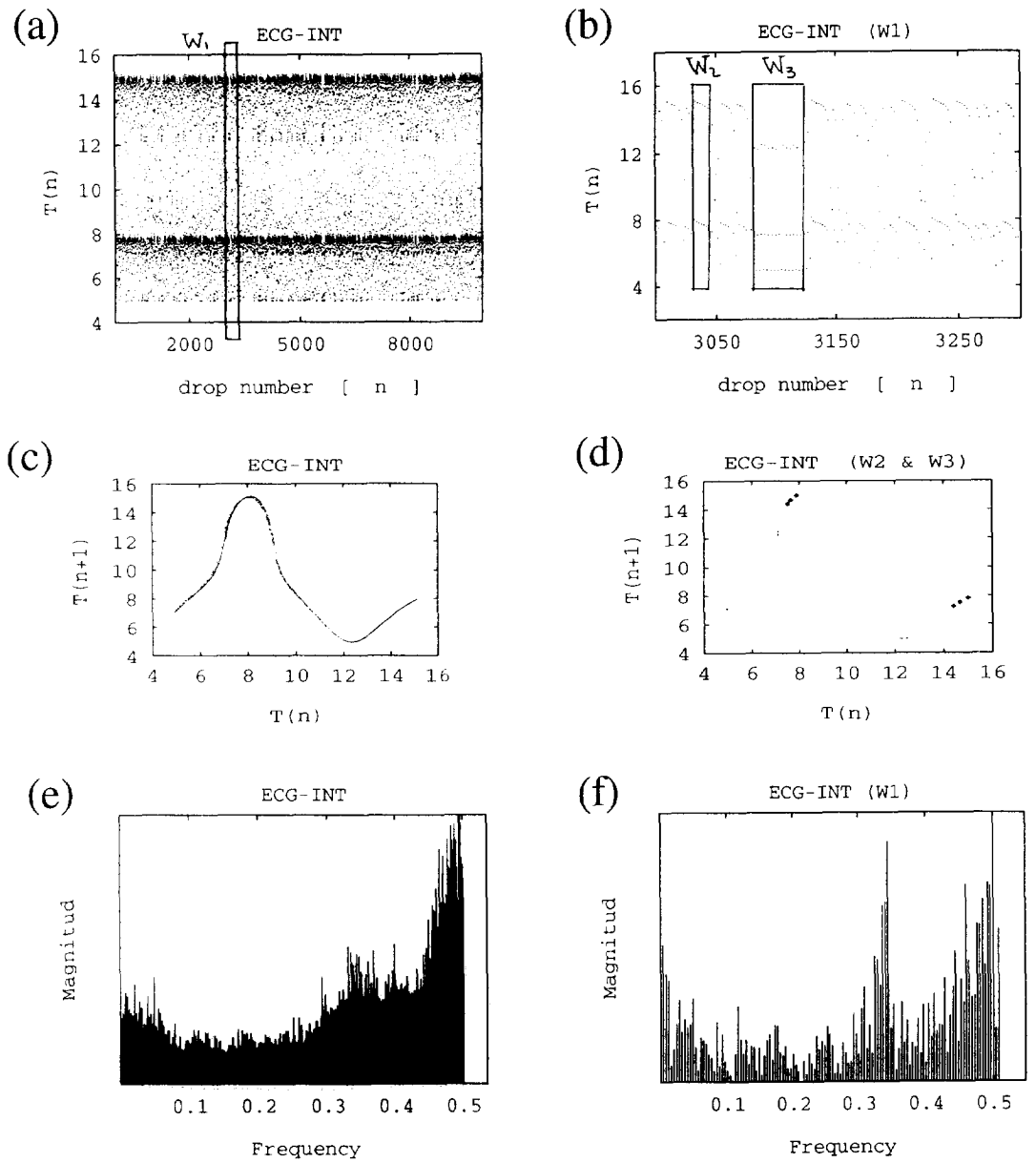

Fig. 10. (a) Series of drip intervals of the attractor ECG-INT. (b) Series of some of the data shown in (a). Notice how the system changes from a period 2 behaviour, to a period 3, period 6 and chaos in brief intervals. (c) Poincaré map of the drip intervals of figure (a). (d) Poincaré map of the data of the period 2 (big dots) and period 3 (small dots) regions of (b). (e) and (f) are the power spectra of data shown in (a) and (b) respectively. The second spectrum emphasizes the peaks of the first at the frequencies $\frac{1}{2}$, $\frac{1}{3}$, $\frac{1}{6}$ among others.

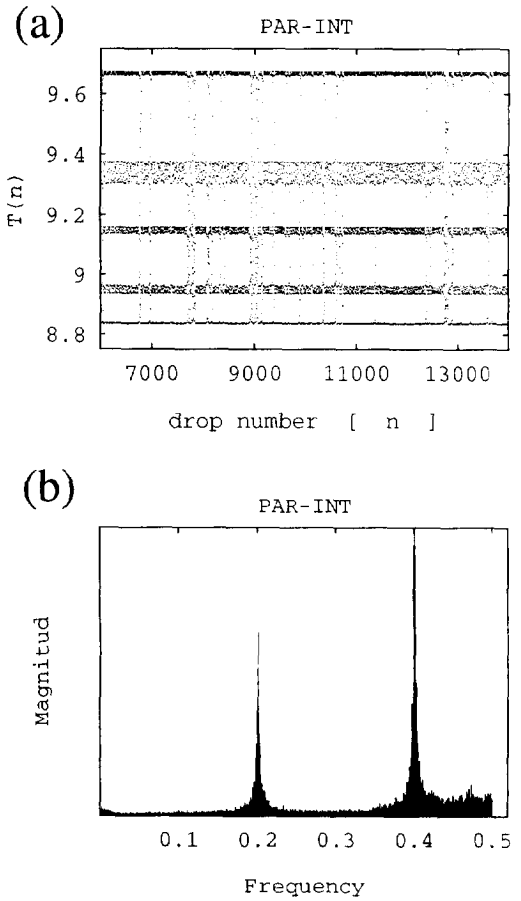

Fig. 11. (a) Series of drip intervals of attractor PAR-INT. (b) Power spectrum of the data of (a). Notice that besides the broad peaks corresponding to the 5 bands of the coarse periodic behaviour, components over the whole range of frequencies reflex the several escapes from those regions.

small drops, and if they are sensitive enough for them, they also count fragments of a drop as several ones [26]. See photographs of the process in [11]). We intend to address this point in the near future by adding simulated noise to the model, and setting a threshold for the mass of the drops.

As we mentioned before, looking at an attractor using reconstructions made of different variables (drip-intervals, masses or velocities) can simplify the characterization of the attractor. We have seen the difference in the complexity for the plots of the hanging mass and the velocity of attractor ECGPAR (Fig. 9). In the case of attractor PAR we found an even more drastic difference between both reconstructions, namely, the apparently abrupt folding of the curve in Fig. 3f. Inspired by the smoothness of reconstructions made from the other variables, we magnified the region of the fold to discover that this was not a sharp joint but a smooth bending. This is a typical example of a characteristic that can be difficult to see when working with one variable and obvious when analysing another one.

After looking at the attractors substructure in magnified plots we expected a somewhat larger value for their dimensions. The values found could have been produced by a mixed behaviour, having parts of the attractor contained on a single line (with Hausdorff dimension less than 1) and some others like those in Fig. 5, pertaining to subsets with an apparent greater dimension (between 1 and 2). At present we are calculating the dimension of several different parts of the attractors with the hope of finding different values for each subset although it seems very likely that this mixed behaviour is in fact present all over the attractor.

Although period doubling is a common feature of both systems, the experiments [12] and the model show that the succession of periods is not strictly ordered (i.e. not monotonously increasing with the variation of the parameters) as one would expect if the system only were following a period-doubling route to chaos (Table 1). On the other hand, both systems exhibit transitions to chaos through tangent intermittence. A further search in the space of parameters is being carried out to clarify the route to chaos (we present some results in [27]). New bifurcation diagrams are being analysed aiming at obtaining a more detailed description of the attractors (like the length of laminar regions) and the critical values of the parameters (when the system abruptly changes its behaviour).

We must realize that the model can be thought of as a coupled harmonic oscillator (Eqs. (1) and (2)) and a relaxation oscillator (Eqs. (3) and (4)), where the solutions to the equations are continuous during each time interval T_n. The analytical solutions can be expressed as a map for the variables T, M, V, and Q between steps n and $n+1$. Such a treatment of the electrical model for the leaky tap [28] has shown

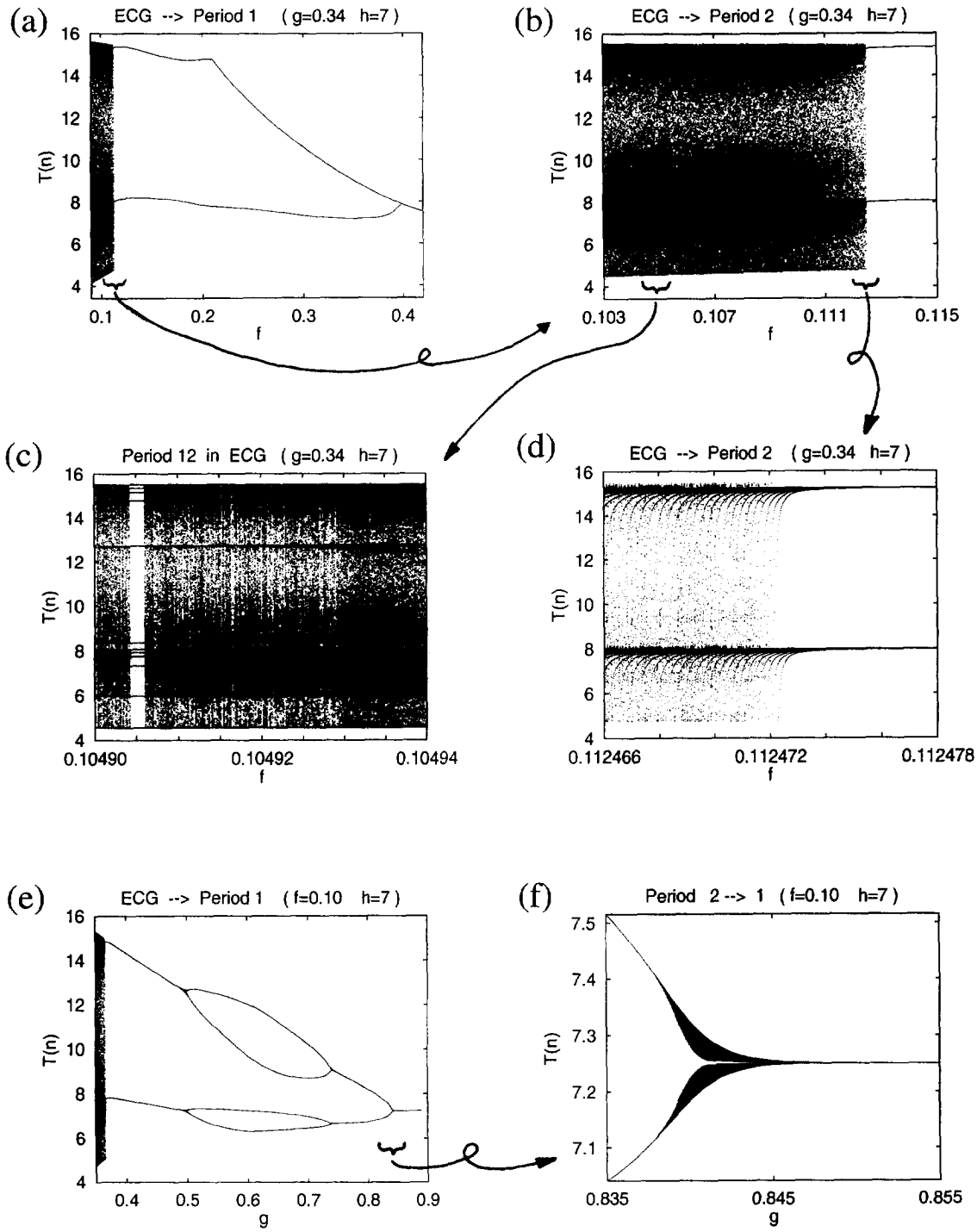

Fig. 12. Bifurcation diagrams. (a) Transition from chaotic attractor ECG to a period 2 and 1 attractors while varying parameter f. (b) Magnification of (a) showing the evolution in the distribution of time intervals as f increases. (c) Blow-up of a section of (b) with a "hole" (a region of f with low dots density), shows that windows with cyclic behaviour of period 12 exist alternated with chaotic attractor ECG. (d) Inspection of the region of (b) where the transition from chaos to the period 2 attractor takes place through tangent intermittence. Like in all bifurcation diagrams presented, dots corresponding to transient states were previously discarded. (e) Transition from chaotic attractor ECG to a period 2, 4, 2 and 1 attractors while varying parameter g. (f) Inspection of a inverse bifurcation shown in (f), where we discard the first 100 time intervals and plot the next 200. Thick parts of the lines show regions were transient states were much longer than 100 drops, and follow a smooth divergent tendency from one to two values.

Table 2
Correlation dimension (D_{corr}), Hausdorff dimension (D_H) and the largest positive Lyapunov exponent (λ_{++}) for some of the reconstructed attractors

Attractor	Data	D_{corr}	D_H	λ_{++} (bits/drop)
PAR ($f = 0.34, g = 0.32, h = 10$)	drip intervals	0.941 ± 0.064	0.994 ± 0.056	0.238 ± 0.023
	masses	0.938 ± 0.069	1.011 ± 0.062	0.245 ± 0.018
ECG ($f = 0.10, g = 0.34, h = 7$)	drip intervals	1.201 ± 0.057	1.236 ± 0.066	0.927 ± 0.021
	masses	1.225 ± 0.069	1.264 ± 0.071	0.928 ± 0.021
ECGPAR ($f = 0.10, g = 0.32, h = 10$)	drip intervals	0.843 ± 0.051	0.955 ± 0.054	0.511 ± 0.038
	masses	0.887 ± 0.053	0.972 ± 0.051	0.539 ± 0.042
ECG-INT ($f = 0.10, g = 0.36, h = 7$)	drip intervals	1.108 ± 0.056	1.140 ± 0.059	0.663 ± 0.025
	masses	1.110 ± 0.058	1.141 ± 0.060	0.674 ± 0.035
PAR-INT ($f = 0.338, g = 0.325, h = 10$)	drip intervals	0.882 ± 0.037	0.905 ± 0.056	0.212 ± 0.031
	masses	0.881 ± 0.040	0.910 ± 0.050	0.230 ± 0.023

a map similar to the twist and flip map described in [29].

Given the rich dynamics found in the model, we continue investigating the system in several areas. At the moment we investigate the map associated to the equations of the variable mass relaxation oscillator presented here. In connection with the succession of unstable periodic motion of chaotic attractors like ECG-INT, we are applying some control concepts to the model and to the real system.

Acknowledgements

It is a pleasure to acknowledge discussions with K. Apu, G. Ubo, M. Ek, C. Cica and F. Ek. G.I.S.-O. wants to thank T.H. Seligman and F. Leyvraz for their enlightening academic advice and irreplaceable help all through this work. GISO also wants to acknowledge the support provided by DGAPA (UNAM) and by CONACYT. He is also grateful to P. Burger for useful remarks and discussions. A.L.S.-B acknowledges the partial support of Fundacion Ricardo J. Zevada and CONACYT under grant 4846-E9406. This paper is dedicated to Professor L. Salas-Canto on the occasion of his birthday.

References

[1] A.V. Holden ed., Chaos (Manchester Univ. Press, Manchester, 1986).
[2] A. Skarda and W.J. Freeman, Behav. Brain Sci. 10 (1987) 161.
[3] H. Hasegawa and S. Adachi, J. Phys. Soc. Jpn. 57 (1988) 80.
[4] E.A. Jackson, Perspectives on Non-linear Dynamics, Vols. I and II (Cambridge Univ. Press, Cambridge, 1990).
[5] H.N. Núñez-Yépez, A.L. Salas-Brito, C.A. Vargas and L. Vicente, Phys. Lett. A 145 (1990) 101;
R. Carretero-González, H.N. Núñez-Yépez nad A.L. Salas-Brito, Eur. J. Phys. 15 (1994) 139;
R. Carretero-González, H.N. Núñez-Yépez and A.L. Salas-Brito, Phys. Lett. A 188 (1994) 48.
[6] W. Lauternborn and J. Holzfuss, Int. J. Bifurcation and Chaos 1 (1991) 13.
[7] G.S. Skinner and H.L. Swinney, Physica D 48 (1991) 1.
[8] R. Shaw, The Dripping Faucet as a Model Chaotic System (Aerial Press, Santa Cruz, USA, 1984).
[9] P. Martien, S.C. Pope, P.L. Scott and R.S. Shaw, Phys. Lett. A 110 (1985) 399.
[10] H.N. Núñez-Yépez, A.L. Salas-Brito, C.A. Vargas and L. Vicente, Eur. J. Phys. 10 (1989) 99.
[11] R.F. Cahalan, H. Leidecker and G.D. Cahalan, Comp. Phys. 3 (1990) 368.
[12] H.N. Núñez-Yépez, C. Carbajal, A.L. Salas-Brito, C.A. Vargas and L. Vicente, in: Non-linear Phenomena in Fluids, Solids and Other Complex Systems, eds. P. Cordero and B. Nachtergaele (Elsevier, Amsterdam, 1991) 467.
[13] X. Wu, Z.A. Schelly, Physica D 40 (1989) 433.
[14] J. Austin, Phys. Lett. A 155 (1991) 148.
[15] P.A. Bernhardt, Physica D 52 (1991) 489; Chaos 2 (1992) 183.
[16] D.N. Baker, A.J. Klimas, R.L. McPherron and J. Buchner, Geophys. Res. Lett. 17 (1990) 41.

[17] J.W.S. Rayleigh, The Theory of Sound (Dover, New York, 1945) 364.
[18] E. Becker, W.J. Hiller and T.A. Kowalewski, J. Fluid Mech. 27 (1991) 189.
[19] C.A. Vargas and A.L. Salas-Brito, Laboratorio de Sistemas Dinámicos UAM-A, unpublished data.
[20] P. Grassberger and I. Procaccia, Phys. Rev. Lett. 50 (1983) 346.
[21] A.M. Oropeza-López, Senior Thesis Dimensión fractal de acelerogramas de sismos registrados en el valle de México (FCUNAM, México D.F., 1991).
[22] A.J. Lichtenberg and M.A. Lieberman, Regular and Stochastic Motion (Springer, Berlin, 1983).
[23] G.I. Sánchez-Ortiz, Senior Thesis El grifo goteante: estudio numérico de un modelo mecánico (FCUNAM, México D.F., 1991).
[24] A. Wolf, J.B. Swift, H.L. Swinney and J.A. Vastano, Physica D 16 (1985) 285.
[25] J.C. Sartorelli, W.M. Gonçalves and R.D. Pinto, Phys. Rev. E 49 5 (1994) 3963.
[26] Z. Néda, B. Bakó and E. Rees, preprint (1994).
[27] G.I. Sánchez-Ortiz and A.L. Salas-Brito, Phys. Lett. A 203 (1995) 300.
[28] P.A. Bernhardt, Int. J. Bifurc. Chaos 4 2 (1994) 427.
[29] R. Brown and L. Chua, Int. J. Bifurc. Chaos 1 1 (1991) 235.